Physical properties of the tetragonal CuMnAs: A first-principles study

F. Máca,* J. Kudrnovský, and V. Drchal
Institute of Physics ASCR, Na Slovance 2, CZ-182 21 Praha 8, Czech Republic

K. Carva, P. Baláž, and I. Turek
Charles University, Faculty of Mathematics and Physics, Department of Condensed Matter Physics, Ke Karlovu 5, CZ-121 16 Praha 2, Czech Republic

(Received 28 June 2017; published 6 September 2017)

Electronic, magnetic, and transport properties of the antiferromagnetic (AFM) CuMnAs alloy with tetragonal structure, promising for the AFM spintronics, are studied from first principles using the Vienna *ab initio* simulation package. We investigate the site occupation of sublattices and the lattice parameters of three competing phases. We analyze the factors that determine which of the three conceivable structures will prevail. We then estimate formation energies of possible defects for the experimentally prepared lattice structure. Mn_{Cu} and Cu_{Mn} antisites as well as Mn $\leftrightarrow$ Cu swaps and vacancies on Mn or Cu sublattices were identified as possible candidates for defects in CuMnAs. We find that the interactions of the growing thin film with the substrate and with vacuum as well as the electron correlations are important for the phase stability while the effect of defects is weak. In the next step, using the tight-binding linear muffin-tin orbital method for the experimental structure, we estimate transport properties for systems containing defects with low formation energies. Finally, we determine the exchange interactions and estimate the Néel temperature of the AFM-CuMnAs alloy using the Monte Carlo approach. A good agreement of the calculated resistivity and Néel temperature with experimental data makes it possible to draw conclusions concerning the competing phases.

DOI: 10.1103/PhysRevB.96.094406

I. INTRODUCTION

The tetragonal antiferromagnetic (AFM) CuMnAs phase prepared by the molecular-beam epitaxy (MBE) on the GaAs(001) and GaP(001) substrates has recently attracted considerable experimental and theoretical interest in connection with so-called AFM spintronics [1–4]. The combined experimental and theoretical study [2] (see also Ref. [5]) has led to a proposal of basic structural parameters that were used in first-principles calculations assuming an ideal structure without defects [2]. On the other hand, the experiment for this phase provides the basic physical parameters: the residual resistivity around 90 $\mu\Omega$cm for $T = 5$ K [2], the Néel temperature around 480 K [6], and the local Mn moments around 3.6 μ_B at room temperature [2]; its value at lower temperature will be higher (see also Sec. III D). The transport studies (the residual resistivity) thus indicate the presence of defects whose origin and concentrations are known only very approximately (sample grown on the GaAs substrate) [5]. Identification of possible defects and their formation energies thus represent a challenge for the theory. The same also concerns an estimate of the residual resistivity and the Néel temperature. The Néel temperature is closely related to corresponding exchange interactions and, in turn, also to the values of local Mn magnetic moments.

Another interesting issue concerns the sample preparation. The CuMnAs in the bulk phase crystallizes in the orthorhombic phase [7] while the studied tetragonal phase does not exist as a bulk phase in nature and can only be prepared as a film by the MBE on a suitable substrate or by separation [8] from an ingot.

The aim of the present study is thus twofold. First, we will determine theoretically the structure of the tetragonal phase by optimizing the lattice parameters ($a = b$ and c in the present case) and positions of Cu, Mn, and As atoms inside the unit cell. We also investigate the effect of the substrate, defects, and of electron correlations [9] on the phase stability. Moreover, we estimate the formation energies of possible defects. Second, we will calculate relevant physical quantities such as the local Mn moments, exchange interactions, and the Néel temperature as well as the residual resistivity due to specific defects. These quantities will be determined in the framework of the unified first-principle electronic structure model and compared with the experiment.

II. FORMALISM

The AFM-CuMnAs prepared by the MBE has a tetragonal structure [2,10] with the space group *P4/nmm* (No. 129) [11]. The experimental lattice parameters are $a = b = 3.82$ Å and $c = 6.318$ Å. The atomic basis contains two formula units (six atoms), Cu atoms are in the basal plane of the tetragonal lattice (Wyckoff position 2*a*), there are two parallel layers of As atoms (Wyckoff position 2*c*), and two layers of Mn atoms (Wyckoff position 2*c*) with oppositely oriented moments (see Fig. 1). The interstitial sites are located in Wyckoff position 2*b*. The relative positions of atoms (in units of c) are $z_{Cu} = 0.0$, $z_{Mn} = u_c = 0.330$, and $z_{As} = v_c = 0.266$.

We call this structure phase I. In the other possible structure, which we call phase II, Mn atoms are in position 2*a*, and Cu and As atoms occupy position 2*c*. Finally, there could be a structure (denoted as phase III) with As atoms in the basal plane (2*a*) and Cu and Mn atoms in position 2*c*.

Theoretical lattice parameters a and c, as well as atomic positions in the unit cell, are determined by VASP calculations

*maca@fzu.cz

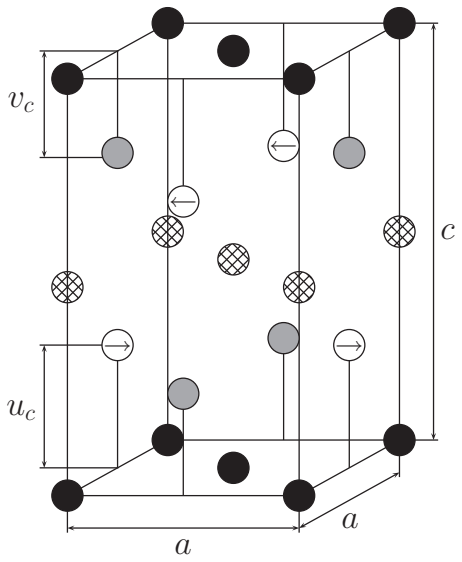

FIG. 1. The lattice structure of phase I of tetragonal AFM CuMnAs consisting of two nonmagnetic Cu/As sublattices (black/grey color), and two Mn sublattices with the antiparallel spin orientations (indicated by arrows). The possible interstitial positions (Wyckoff position 2*b*) are shown by hatched circles. For phase II, the positions of Cu and Mn atoms are interchanged.

(Vienna *ab initio* simulation package using the projector augmented wave scheme [12]) with different exchange correlation potentials, namely, the LDA (Vosko-Wilk-Nusair, VWN) [13], the GGA (Perdew-Burke-Ernzerhof, PBE) [14], and the GGA+U with a simple empirical on-site Coulomb interaction U related to Mn d-orbitals [15]. The supercell VASP calculations (48 atoms) are used to determine formation energies of possible simple defects assuming the experimental lattice structure. For VASP calculations, we have used plane waves up to 350 eV and the Brillouin zone sampling with 270 special k-points in the irreducible three-dimensional wedge and corresponding number of k-points in the supercell.

The transport coefficients, exchange interactions, and the Néel temperature are determined using the Green function formulation of the tight-binding linear muffin-tin orbital (TB-LMTO) method in which the effect of disorder (defects) is described by the coherent potential approximation (CPA) [16]. The TB-LMTO method employs the atomic sphere approximation and is thus less accurate than the VASP technique. We have therefore compared relevant electronic properties [local moments and densities of states (DOS)] with the VASP results for the ideal, defect-free AFM-CuMnAs assuming the experimental structure. This is an important check for more complex, noncubic structures (see, e.g., Ref. [17]). Calculations are done using the VWN exchange-correlation potential, but we also check the robustness of the result with respect to the electron correlations (on-site Coulomb interaction model). We have neglected the spin-orbit effects in both approaches.

The transport studies employ the Kubo-Greenwood linear response theory in which the disorder-induced vertex-corrections are included in the CPA [18]. Their inclusion is simplified by the present formulation of the velocity as the intersite hopping [19], which leads to nonrandom velocity matrices.

The effective exchange interactions between Mn atoms for a given shell s, J_s, are determined by the Liechtenstein mapping procedure [20] generalized to random alloys [21]. As a result, we obtain the effective Heisenberg Hamiltonian $H = -\sum_{ij} J_{ij}\mathbf{e}_i \cdot \mathbf{e}_j$, which will be used for the estimate of the Néel temperature. The indices i and j run over all sites occupied by Mn atoms, J_{ij} denote the pair exchange interactions, and the unit vectors $\mathbf{e}_i$ define the local moment directions. We note that the positive/negative values of J_s correspond to the ferromagnetic (FM)/AFM interactions and that the values of magnetic moments are included in their definitions [20,21]. The exchange interactions depend on the reference magnetic state from which they are extracted. In particular, in the present case we employ two reference states, namely, the AFM state and the disordered local moment (DLM) state [22]. The DLM approach describes the paramagnetic state above the critical temperature with fluctuating Mn moments and is thus better suited for the estimate of the critical (Néel) temperature for the transition between the AFM and paramagnetic states as compared to the AFM reference state corresponding to zero temperature. The DLM state is treated as a random equiconcentration binary alloy of moments pointing randomly in opposite directions and can be thus naturally treated using the CPA [22]. In both cases, however, local moments on Cu and As atoms are strictly zero. It should be noted that, due to the two Mn sublattices, we will have two sets of exchange parameters, intra- and intersublattice ones. We remark that the DLM state will be also used in transport studies.

To study the thermodynamic properties of CuMnAs, we employed classical Monte Carlo (MC) simulations based on the Metropolis algorithm [23] applied to the constructed Heisenberg Hamiltonian. For simulations, we used a three-dimensional supercell composed of $16 \times 16 \times 16$ elementary CuMnAs cells with periodic boundary conditions. The simulations were carried out assuming zero applied magnetic field and disregarding magnetocrystalline anisotropy. The local Mn magnetic moments, as large as $3.80\,\mu_B$, were assumed to be independent of temperature. We started the simulation from an initial temperature 900 K, which decreased by a step $\Delta T = 10$ K. At each temperature, 2×10^5 MC steps were performed. To accumulate the statistics, we simultaneously simulated five independent identical systems.

III. RESULTS AND DISCUSSION

A. Ground state of the ideal tetragonal AFM-CuMnAs

Assuming the ideal tetragonal AFM-CuMnAs, two natural questions arise: (i) the occupation of atomic positions inside the elementary cell by Cu, Mn, and As atoms, i.e., which phase (I, II, or III) corresponds to the ground state; and (ii) optimal lattice parameters $a = b$, and c and the coordinates of atoms inside the unit cell. This structure allows both the FM alignment (e.g., in CrMnAs [10]) and the AFM alignment (like in CuMnAs), but also more complex magnetic structures could exist if one considers larger unit cells, but here we limit ourselves to the case of six atoms per unit cell observed in the experiment [2].

TABLE I. Total energies per elementary cell of phase II with respect to phase I (energy zero) are shown assuming the (frozen) experimental geometry (label 0) as well as the optimized one. Also shown are lattice parameters a, c, the relative z coordinates of Cu, Mn, As atoms inside the unit cell, its volume V, and the local Mn-moments m^{Mn}. In the bottom part of the table, the nearest-neighbor distances between various atom pairs in all structures are given.

	Phase I_0	Phase I	Phase II_0	Phase II
a [Å]	3.82	3.69	3.82	3.85
c [Å]	6.32	6.40	6.32	5.94
V [Å^3]	92.20	87.14	92.20	88.05
z_{Cu}	0.00	0.00	0.670	0.682
z_{Mn}	0.670	0.651	0.00	0.00
z_{As}	0.266	0.273	0.266	0.270
m^{Mn} [μ_B]	3.70	3.41	2.96	2.78
ΔE_{tot} [eV]	0.0	0.0	−0.078	−0.102
$d_{\mathrm{Cu-Cu}}$ [Å]	2.70	2.61	3.45	3.48
$d_{\mathrm{Cu-Mn}}$ [Å]	2.82	2.90	2.82	2.70
$d_{\mathrm{Cu-As}}$ [Å]	2.55	2.54	2.55	2.74
$d_{\mathrm{Mn-As}}$ [Å]	2.55	2.66	2.55	2.51
$d_{\mathrm{Mn-Mn}}$ [Å]	3.45	3.24	2.70	2.72
$d_{\mathrm{As-As}}$ [Å]	3.82	3.69	3.82	3.85

Results of extensive calculations in the framework of the VASP and GGA-PBE are summarized in Table I for the optimized phases I and II together with distances between atoms. We have also included results for the experimental geometry [2].

The following conclusions are made: (i) The ground state is phase II, but with the energy preference with respect to phase I being only about 0.1 eV per unit cell. The lattice parameter c is about 6% smaller as compared to the grown sample, while the lattice parameter a is similar; (ii) In phase I, the result is just the opposite: The lattice parameter c is similar to that in the grown sample, but the lattice parameter a is smaller by 3.5%; (iii) Theoretical volumes for phases I and II were smaller as compared to the experimental one, thus indicating a possible role played by the substrate; (iv) The energy preference of phase II as compared to phase I (by about 0.08 eV per unit cell) is obtained also for the experimental structure; (v) The values of local Mn moments are strongly underestimated in both phases II and III as compared to the experiment; and (vi) The total energy of phase III (with As atoms in the basal plane) was estimated for the experimental lattice parameters, but with optimized atom positions. It was higher than that of phase I by 2.97 eV. Calculated interatomic distances among atoms (Table I) also indicate a possible experimental test—using the Extended X-ray Absorption Fine Structure experiment, which could distinguish between possible phases, namely, by checking the nearest-neighbor Mn-Mn distances which differ significantly and do not interfere with distances between other atom pairs. Additional arguments in favor of phase I will be given below based on the transport studies and an estimate of the Néel temperature.

For phase I at the experimental geometry, we have also estimated total energies of the FM and nonmagnetic CuMnAs phases (+0.29 eV and +2.82 eV), respectively. Corresponding total energies are higher as compared to the AFM total energies so that they can be excluded as possible ground state candidates. On the other hand, the energy difference between the AFM and FM states is smaller for phase II as compared to phase I (+0.069 eV and +0.29 eV, respectively). Such a result is compatible with exchange interactions of both phases I and II, namely with dominating AFM interactions for the former and competing FM and AFM interactions for the latter [see Figs. 4(b) and 4(c) below].

TABLE II. Total energy differences (per elementary cell) between phases I_0 and II_0, $\Delta E_{\mathrm{tot}} = E_{\mathrm{II}_0} - E_{\mathrm{I}_0}$, as a function of the on-site Hubbard parameter U. Also shown are corresponding local Mn moments.

U [eV]	0	0.41	0.83	1.25
$m^{\mathrm{Mn}}_{I_0}$ [μ_B]	3.70	3.80	3.90	3.99
$m^{\mathrm{Mn}}_{II_0}$ [μ_B]	2.96	3.15	3.31	3.46
ΔE_{tot}[eV]	−0.078	+0.102	+0.278	+0.443

While the semilocal GGA exchange-correlation potential is generally considered to be an optimal choice for the structure optimization, the GGA+U approach is sometimes used to find the theoretical description in some systems, tuning of band gaps, magnetic moments, the critical temperatures, etc. (see, e.g., a recent study of the AFM MnTe) [9]. We present here a similar study of the effect of electron correlations on the lattice structure and magnetic moments in the AFM-CuMnAs assuming that the Hubbard parameter U is limited to d orbitals of Mn atoms, which is an acceptable model for narrow Mn bands (Table II).

Electron correlations stabilize phase I_0 as compared to phase II_0. Already for $U = 0.4$ eV, phase I_0 has a lower total energy than phase II_0. Assuming U around 1 eV, the local Mn moment (3.9−4.0 μ_{B}) also agrees reasonably well considering that it was measured at room temperature. We have also tested the effect of lattice relaxations and found only slight quantitative modifications not changing the qualitative picture.

There are two other effects which could influence the calculated phase stability, namely, that samples are grown on the particular substrate and the presence of impurities in the sample. The real samples are grown on the As-/P-terminated GaAs(001)/GaP(001) faces [24]. We have tried to elucidate a possible role of the substrate using a simple model which simulates this case, namely, the system consisting of five layers of GaP simulating the substrate with an extra layer of P atoms (P-rich conditions) which interface with four multilayers of CuMnAs, either in phase I (the bottom layer is Cu one) or in the phase II structure (the bottom layer is Mn one). Such a system separated by a vacuum layer is periodically repeated and studied by the supercell method. We used the VASP-GGA, fixed the substrate layers, but allowed relaxation of an extra layer of P atoms, and atoms inside CuMnAs. We also varied spin orientations—the AFM orientation was either between Mn layers or inside each Mn layer. In all cases, the AFM orientation between Mn layers was preferred. Finally, we have also tested models with frozen experimental sample geometry. In all cases, we have obtained the preference of phase I; the

TABLE III. The formation energies FE for various substitutional defects in the tetragonal AFM-CuMnAs. Also studied was the Mn interstitial (Mn_{int}, see Fig. 1). The symbol X_Y denotes the X defect on the Y sublattice. Defects are sorted according to their formation energies; the values for unrelaxed atom positions are given in parenthesis.

Defect	FE [eV]	Defect	FE [eV]
Vac_{Mn}	−0.13 (−0.23)	Mn_{int}	+1.62 (+2.15)
Vac_{Cu}	−0.13 (−0.10)	As_{Cu}	+1.73 (+2.66)
Mn_{Cu}	−0.04 (−0.06)	As_{Mn}	+1.77 (+1.90)
Cu_{Mn}	+0.33 (+0.27)	Mn_{As}	+2.00 (+1.95)
Cu_{As}	+1.15 (+1.06)	Vac_{As}	+2.18 (+2.22)

energy difference in its favor was quite substantial and varied between 0.8 and 1 eV per elementary cell with 42 atoms.

The present model fulfills the basic requirement for comparison of total energies, namely, the same number of atoms in supercells. The model correctly includes sample/vacuum and sample/substrate interfaces as it is in a real system. On the other hand, it has certain limitations as we do not consider possible switching between phases I and II during the growth. One should keep in mind that theoretical calculations assume zero temperature and give the global minimum of energy, while a real sample exists in a nonequilibrium state due to sample preparation and it can be in the local energy minimum.

We refer the reader to the end of the next section as concerns a possible effect of impurities on the phase stability.

B. Formation energies of defects in AFM-CuMnAs

Structural study [5] and measurements of residual resistivity (90 $\mu\Omega$cm) indicate that the samples contain defects. An estimate of the formation energies (FE) of defects is a tool that can identify possible candidates. A complete study of all possible defects, similar to that done for a cubic FM-NiMnSb [25] is beyond the scope of the present paper. Rather, we choose a few possible candidates as in the study for related CuMnSb alloy [26]. We have estimated FE for chosen substitutional defects including vacancies, as well as for Mn interstitial, and listed them in Table III.

The supercell VASP method and GGA-PBE was applied to the referenced 48-atom supercell $Cu_{16}Mn_{16}As_{16}$ and to corresponding supercells containing specific defects. For example, $Cu_{15}Mn_{17}As_{16}$ supercell simulates the Mn_{Cu} defect concentration of 6.25%. We have used the experimental lattice parameters. The accurate determination of FE is a challenging task (see, e.g., a recent review [27]). Here we employ the simplest possible approach in which the FE is defined as $FE = E_{tot}[def] - E_{tot}[id] - \sum_i n_i E_i$, where $E_{tot}[def]$ and $E_{tot}[id]$ are total energies of the supercells with (def) and without (id) defects, n_i indicates the number of atoms of type i (i = Cu, Mn, As, vacancy) that have been added to ($n_i > 0$) or removed from ($n_i < 0$) the supercell when the defect is formed, and E_i are total energies of atoms in their most probable bulk phase [27]. Strictly speaking, instead of E_i, one should employ corresponding chemical potentials of these species, which may depend on the temperature, defect concentration, the presence of other defects, etc. The above choice represents a rough, but acceptable approximation. It was used, e.g., in Refs. [25,26] for cubic semi-Heusler NiMnSb and CuMnSb alloys. We have chosen for E_i the total energies of fcc-Cu, AFM-Mn ($L1_0$-lattice), and rhombohedral As. The choice for Mn is the same as in Ref. [25], although, in the OQMD (Open Quantum Materials Database [28]), a more complex structure is used [29]. It should be noted that actual values for the FE may depend on the choice of these energies and on the determination of $E_{tot}[def]$. While the lattice parameters (a, c) were kept fixed in all cases, we have optimized atomic positions inside the supercell. We have also tested the model with frozen atomic positions like in the ideal structure, but there were only small quantitative differences. Results are summarized in Table III with the following conclusions: (i) Mn_{Cu} and Cu_{Mn} are, similarly, as in the cubic CuMnSb, the most probable candidates for possible defects. In addition, vacancies on Mn and Cu sublattices have small FE. We note that a small FE for Mn vacancy [25] was also found for NiMnSb alloy; (ii) Mn interstitials have, contrary to CuMnSb or NiMnSb, a much larger FE due to tetragonal vs cubic structure with natural vacancy sites in the latter; (iii) Also Mn_{As} or As_{Mn} and related defects have large FE similar to Mn_{Sb} and Sb_{Mn} in NiMnSb or CuMnSb [25,26]; and (iv) Although the FE of Mn ↔ Cu swaps was not explicitly studied, one can roughly estimate it as the sum of FE of Mn_{Cu} and Cu_{Mn}, assuming that they are not correlated [26]. Consequently, the Mn ↔ Cu swaps are also possible candidates. To resume, we regard the defects with FE in tenths of eV as probable, while those with FE above 1 eV we do not further consider.

Essentially zero (small negative) FE for Mn-Cu swap correlates with the fact that corresponding total energies of phases I and II have very similar energies (see Table I), phase II has the total energy even slightly lower. Besides the FE, the formation of defects depends on delicate details of the impurity kinetics, which is not considered here. Anyway, defects with low FEs are more probable candidates than those with larger FEs even at the nonequilibrium conditions. We will therefore investigate below the influence of these more probable defects on transport properties. It should be noted that defects play a less important role on the value of the Néel temperature as compared to the resistivity, so that we limit ourselves to defect-free samples when calculating Néel temperature.

We have further studied the possible effect of impurities on the phase stability. We have taken two defect types with low and high formation energies (see below), namely Mn_{Cu} and Mn_{As}, and also investigated the effect of the defect concentrations (supercells simulating the defect concentrations 6.25% and 12.5%, respectively). Neither the defect type nor the higher defect concentration were able to change the energy preference of phase II.

C. Transport properties of AFM-CuMnAs

We will estimate residual resistivities due to possible defect types found in the previous section, namely, Mn_{Cu}, Cu_{Mn}, Mn vacancy, and Mn ↔ Cu swap, assuming the defect concentration of 5% in each case.

To this end we employ the linear-response theory as formulated in the TB-LMTO-CPA method [19], including

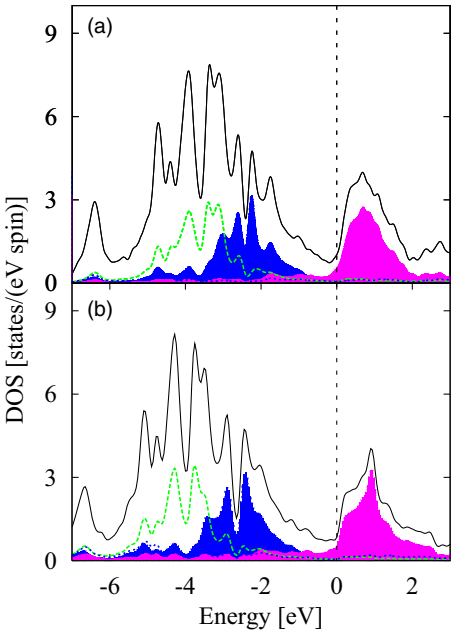

FIG. 2. Comparison of total and local densities of states (DOS) for the phase I of AFM-CuMnAs alloy evaluated using (a) VASP method and (b) the TB-LMTO method in the LDA framework. The spin-resolved local Mn-DOS are shown (majority spin—blue, minority spin—red). The local Cu (dashed line) and As DOS (dotted line) are spin-independent.

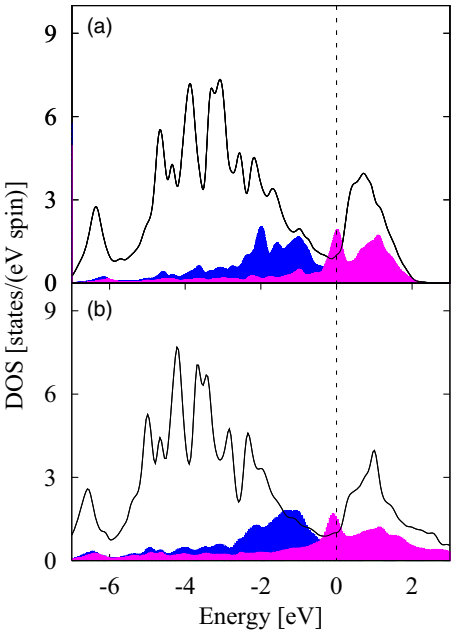

FIG. 3. The total and local densities of states (DOS) for the reference AFM-CuMnAs alloy with 5% of extra Mn atoms on Cu sublattices (a) VASP result, (b) LMTO. We show only the local Mn-DOS on Cu sublattice (majority spin—blue, minority spin—red) to show the pronounced virtual bound state at the Fermi energy in minority states.

disorder-induced vertex-corrections [18], and neglect possible relativistic effects (spin-orbit interaction) for simplicity.

We will first demonstrate that the present tetragonal AFM-CuMnAs alloy can be described properly by the TB-LMTO method similarly as we did recently [17] for topological insulator Bi_2Te_3. Careful tests have led to the conclusion that we can use a model without empty spheres and assuming the same atomic Wigner-Seitz radii. We present in Figs. 2(a) and 2(b) the DOSs for an ideal tetragonal AFM-CuMnAs as calculated by the VASP and TB-LMTO methods, respectively, using the VWN exchange-correlation potential in both cases. A very good agreement between both DOSs is obtained. A similarly good agreement was also obtained for phase II and for models with empirical Hubbard U (not shown).

Concerning the transport properties, there is an important difference between Mn_{Cu} defects or Mn $\leftrightarrow$ Cu swaps on one side and Cu_{Mn} defects or Mn vacancies on the other hand. First, the frustration of the Mn_{Cu} moments is obvious (see Fig. 1). We have therefore considered two limiting models: (i) Collinear moment alignments, both the parallel or antiparallel (P/AP) to the nearest native Mn sublattices, which have the same total energy, and (ii) the DLM state applied to Mn_{Cu} moments characterizing an ideal frustrated state. We have found (5% defects) that the total energy for the DLM-Mn_{Cu} is smaller by a negligible 0.17 meV per formula unit. Second, a virtual bound state (VBS) is present at the Fermi energy for Mn_{Cu} and Mn $\leftrightarrow$ Cu swap defects and it is missing for Cu_{Mn} defects or Mn vacancies.

The VBS in the DOS for Mn_{Cu} defect is shown in Figs. 3(a) and 3(b) for the VASP and TB-LMTO methods, respectively. We have assumed the DLM-Mn_{Cu} model for the TB-LMTO while, for the VASP, we again used 48-atom supercell with a single Mn atom on the Cu site (the concentration 6.25%). It should be noted that a similar VBS was found in the TB-LMTO approach, also for the collinear P/AP model, and/or for the Mn $\leftrightarrow$ Cu swap model (not shown). The presence of impurity states at the Fermi energy will lead to a stronger scattering due to the VBS (Mn_{Cu} or Mn $\leftrightarrow$ Cu defects) and thus larger resistivity (for a comparable defect concentrations) as compared to the Cu_{Mn} defect or Mn vacancy.

We have verified that the VBS exists at the Fermi energy and also for the LDA+U model. The final remark is related to the transport geometry, namely, to the fact that the current can flow either in the (x,y)-plane (in-plane current), used in the experiment, or normal to it, i.e., in the z-direction (out-of-plane current). We have summarized some typical results for different defects in Table IV.

The following conclusions can be drawn: (i) The resistivity in the z direction for all models (the ρ_{zz} component) is much larger than that in the (x,y) plane; (ii) The in-plane resistivity for the DLM state is more symmetric, i.e., ρ_{xx} and ρ_{yy} components are the same while, for the collinear P/AP alignment, they are different, because the presence of ordered moments on a nonmagnetic sublattice lowers the symmetry of the system; (iii) Resistivities roughly follow linear concentration dependence, so one can say that defect concentrations between 3.5% to 5% can reproduce the experimental (planar) resistivity of 90 $\mu\Omega$cm for Mn_{Cu} or Mn $\leftrightarrow$ Cu swap defects while much larger defect concentrations are needed for Cu_{Mn} defects or Mn vacancies (no VBS state at the Fermi energy); (iv) The resistivity for Mn $\leftrightarrow$ Cu swaps is slightly larger as compared to that for Mn_{Cu} defect for the same defect concentrations due to

TABLE IV. The calculated resistivities (in $\mu\Omega$cm) for tetragonal AFM-CuMnAs with 5% of different defect types (models A to G). The resistivity of the paramagnetic state (SDR) is also shown (Model G). The experimental values for the sample with unspecified amount of defects [2] are about 90/160 $\mu\Omega$cm as measured at temperatures $T = 5$ K/300 K, respectively.

	Model	ρ_{xx}	ρ_{yy}	ρ_{zz}
A	P/AP-Mn_{Cu}	104	71	147
B	DLM-Mn_{Cu}	111	111	171
C	P/AP-Mn $\leftrightarrow$ Cu swap	124	97	267
D	DLM-Mn $\leftrightarrow$ Cu swap	124	124	287
E	Cu_{Mn}	24	24	121
F	Mn vacancies	36	36	155
G	SDR for Mn_{Cu}	234	234	363

extra scattering at Cu_{Mn} defects forming the Mn $\leftrightarrow$ Cu swap. The Matthiessen rule is violated, namely, the sum of resistivity for models B and E is $\rho_{xx} = 135$ $\mu\Omega$cm while for Model D it is 124 $\mu\Omega$cm; and (v) The effect of vertex corrections is small.

We have also tested the effect of electron correlations in LDA+U model. As an example, we have chosen Model B and the Hubbard parameter $U = 2$ eV. Calculated resistivity components are larger due to the larger scattering on Mn_{Cu} defects, which, in turn, is due to the increase of the local Mn moments caused by correlations. For example, for Model B we have an increase of ρ_{xx} by about 18 $\mu\Omega$cm, or by 15%. We have also considered phase II. As an example, we have again calculated resistivity for Model B. The resistivity is smaller ($\rho_{xx} = 42$ $\mu\Omega$cm vs 111 $\mu\Omega$cm for the phase I case) due to the smaller effective scattering (smaller local Mn_{Cu} moments).

As an example of the effect of temperature on transport properties, we have calculated [30] the resistivity in the paramagnetic (DLM) state above the Néel temperature [often called the spin-disorder resistivity (SDR)]. The experiment [2] indicates a large increase of the planar resistivity from about 90 $\mu\Omega$cm at 5 K to about 160 $\mu\Omega$cm at 300 K. Such a large increase cannot be ascribed only to phonons (e.g., a phonon contribution to the resistivity of about 25 $\mu\Omega$cm exists for bcc-Fe at the Curie temperature $T = 1050$ K). The largest part of contribution to the resistivity of bcc-Fe should be ascribed to spin fluctuations. To illustrate the effect for CuMnAs as well, one can compare Model B (Mn impurity on Cu with the spin disorder decribed by the DLM state) and Model G describing the paramagnetic state (SDR) in which the spin disorder exists also on the native Mn sublattices. The calculated SDR is around 230 $\mu\Omega$cm, which looks reasonable because the temperature of measurement (300 K) is appreciably smaller than the Néel temperature (480 K). The contribution due to spin fluctuations monotonically increases with temperature up to the Néel temperature and then remains constant so that the calculated SDR seems reasonable.

The resistivity depends on the actual occupation of sublattices, which is a challenging problem connected with similar scattering crossections of atoms forming the alloy. In Ref. [5] for a sample grown on GaAs(001), it was suggested that the Cu lattices are fully occupied by Cu atoms while 8% of Cu and 8% of Mn atoms are found on the As sublattice, leaving about 14% vacancies on the Mn sublattice. A recent analysis [31] for a sample grown on GaP(001) as in Ref. [2] has indicated the presence of 10% vacancies on both the Cu and Mn lattices. It should be emphasized that actual compositions should not be taken literally as they depend on the annealing and can also slightly fluctuate from sample to sample. Calculated longitudinal resistivities for GaAs and GaP grown samples are about 180 $\mu\Omega$cm and 88 $\mu\Omega$cm, respectively, indicating a better agreement with the experiment [2] for samples grown on GaP.

D. Exchange interactions and the Néel temperature

The exchange interactions in the ideal (defect-free) phase I for both AFM- and DLM- (paramagnetic) reference states are shown in Figs. 4(a) and 4(b), respectively, while the corresponding interactions for phase II and assuming the DLM-reference state are shown in Fig. 4(c). In all cases we show interactions among atoms on the same Mn sublattice (intrasublattice interactions) as well as among atoms on different Mn sublattices (intersublattice interactions). All other interactions are zero. The following conclusions can be done: (i) Exchange interactions for the AFM reference state exhibit, as expected, a strong leading AFM intersublattice coupling while the intrasublattice ones are much smaller in their absolute values; (ii) More important are interactions derived from the paramagnetic (DLM) state. The paramagnetic state assumes no specific magnetic order and the character of such interactions is a precursor of the possible AFM ground state (see also Ref. [26]). The fact that qualitative character of both intersublattice and intrasublattice interactions is the same as in the AFM reference state can be interpreted as a strong indication of the AFM ground state; and (iii) Because dominating (AFM-like) intersublattice interactions in the paramagnetic state are smaller than those derived from the AFM reference state, one can expect a lower Néel temperature derived from the DLM state. We have also estimated exchange interactions for the paramagnetic state for phase II, which are shown in Fig. 4(c). The interactions are very different, in particular the intersublattice ones. Consequently, one can expect a very different Néel temperature.

The Néel temperatures were determined using the atomistic spin dynamics (ASD) codes [32], which contain the package for the estimate of critical temperatures using the Monte Carlo simulations. We show in Fig. 5 the sublattice magnetizations and the heat capacity as a function of the temperature. The sublattice magnetizations at $T = 0$ K (equal to the local Mn moments) are reduced with temperature due to spin fluctuations and disappear at the Néel temperature. An internal test of consistency of calculations is that temperature dependence of both sublattice magnetizations should be identical and they indeed are. The magnetization at the Néel temperature is not zero, but rather smeared out due to the finite size of sampling supercells used in the MC calculations. It should be noted, however, that the zero sublattice magnetizations do not mean that local moments are also zero. On the contrary, the local Mn moments in the AFM and DLM states are very similar due to the rigidity of Mn moments, with respect to their rotations. The Néel temperature can be more precisely extracted from the maximum of the heat capacity [see Fig. 5(b)]. The Néel

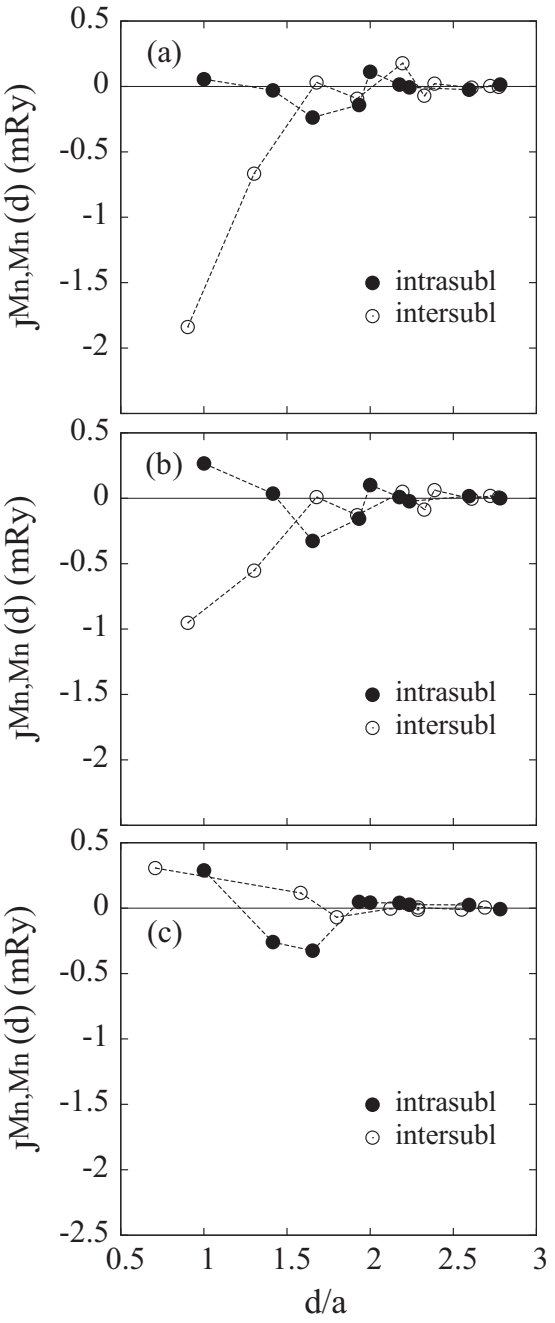

FIG. 4. Exchange interactions for the tetragonal CuMnAs between Mn atoms as a function of the distance d (in units of the lattice constant a): (a) Phase I, AFM state, (b) Phase I, paramagnetic (DLM) state, and (c) Phase II, DLM state. The exchange interactions are subdivided into two groups, namely, between Mn atoms on the same sublattice (intrasubl) and between atoms on different sublattices (intersubl).

temperature estimated in this way and employing exchange interactions derived from the paramagnetic (DLM) reference state is about 480 K [33]. This represents a good agreement of calculated and experimental Néel temperatures, considering that we have assumed an ideal, defect-free phase I while the real sample [6] contains an unspecified amount of defects. The estimated Néel temperature for the AFM reference state is

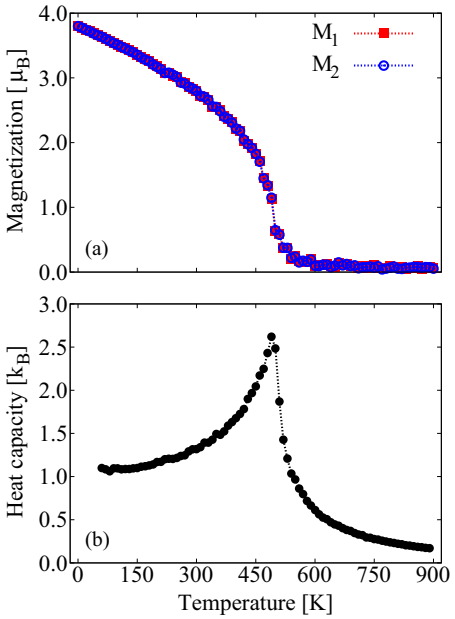

FIG. 5. (a) Magnetizations of the Mn sublattices as a function of temperature assuming exchange interactions derived from the paramagnetic (DLM) state of the tetragonal CuMnAs with the phase I structure. By symmetry, the dependence of both sublattice magnetizations on the temperature is the same. (b) The temperature dependence of the heat capacity from which the Néel temperature can be extracted more accurately (about 480 K).

higher, being about 680 K, as expected from larger values of exchange interactions [Fig. 4(a) vs Fig. 4(b)]. Finally, we have obtained a paramagnetic state using the exchange interactions corresponding to the DLM reference state and phase II [see Fig. 4(c)]. On the basis of this result, one can exclude phase II as a ground state.

IV. CONCLUSIONS

We have performed an extensive *ab initio* study of electronic, magnetic, and transport properties of the tetragonal AFM-CuMnAs alloy with potential technological applications. The VASP approach was used for the phase stability and the estimate of formation energies of possible defects. In the next step, for the experimental lattice structure, the TB-LMTO-CPA approach was adopted to estimate transport properties and the Néel temperature from calculated exchange interactions by the Monte Carlo method. The main conclusions are: (i) The theoretical optimized structure of the bulk tetragonal AFM-CuMnAs is the phase II, but with smaller volume than the experimental one. The same result was obtained for the experimental lattice parameters and optimized atomic positions inside the unit cell; (ii) We have found that electron correlations stabilize phase I; (iii) There are indications that the presence of the substrate favors phase I; (iv) The presence of various defects—even at higher concentrations—does not change the phase preference; (v) Mn_{Cu}, Cu_{Mn}, Mn $\leftrightarrow$ Cu swaps, and vacancies on Mn and Cu sublattices are defects with low formation energies and thus probable candidates that can explain the finite sample resistivity; (vi) Estimated

in-plane resistivity of CuMnAs systems with Mn_{Cu} defects and Mn ↔ Cu swaps for concentrations around 3.5–5% explains experimentally observed values while much larger concentrations would be needed for Cu_{Mn} defects or Mn vacancies. The origin of larger resistivity can be ascribed to the existence of the well-pronounced virtual bound state at the Fermi energy for Mn_{Cu} defect or Mn ↔ Cu swap; and (vii) Estimated Néel temperature for ideal, defect-free AFM-CuMnAs agrees reasonably well with the experiment, keeping in mind that sample contains an unspecified amount of defects. On the other hand, the ideal phase II gives a paramagnetic state which contradicts experimental findings.

ACKNOWLEDGMENTS

We acknowledge the financial support from the Czech Science Foundation (Grant No. 14-37427G) and the National Grid Infrastructure MetaCentrum (Project No. LM2015042) for access to computation facilities.

[1] T. Jungwirth, X. Marti, P. Wadley, and J. Wunderlich, Nat. Nanotech. **11**, 231 (2016).
[2] P. Wadley, V. Novák, R. P. Campion, C. Rinaldi, X. Martí, H. Reichlová, J. Zelezný, J. Gazquez, M. A. Roldan, M. Varela, D. Khalyavin, S. Langridge, D. Kriegner, F. Máca, J. Mašek, R. Bertacco, V. Holý, A. W. Rushforth, K. W. Edmonds, B. L. Gallagher, C. T. Foxon, J. Wunderlich, and T. Jungwirth, Nat. Commun. **4**, 2322 (2013).
[3] P. Wadley, B. Howells, J. Zelezný, C. Andrews, V. Hills, R. P. Campion, V. Novák, K. Olejnik, F. Maccherozzi, S. S. Dhesi, S. Y. Martin, T. Wagner, J. Wunderlich, F. Freimuth, Y. Mokrousov, J. Kuneš, J. S. Chauhan, M. J. Grzybowski, A. W. Rushforth, K. W. Edmonds, B. L. Gallagher, and T. Jungwirth, Science **351**, 587 (2016).
[4] L. Smejkal, T. Jungwirth, and J. Sinova, Phys. Status Solidi Rapid Res. Lett. **11**, 1700044 (2017).
[5] P. Wadley, A. Crespi, J. Gázquez, M. A. Roldán, P. García, V. Novák, R. Campion, T. Jungwirth, C. Rinaldi, X. Martí, V. Holý, C. Frontera, and J. Rius, J. Appl. Cryst. **46**, 1749 (2013).
[6] V. Hills, P. Wadley, R. P. Campion, V. Novák, R. Beardsley, K. W. Edmonds, B. L. Gallagher, B. Ouladdiaf, and T. Jungwirth, J. Appl. Phys. **117**, 172608 (2015).
[7] F. Máca, J. Mašek, O. Stelmakhovych, X. Marti, K. Uhlírová, P. Beran, H. Reichlová, P. Wadley, V. Novák, and T. Jungwirth, J. Magn. Magn. Mater. **324**, 1606 (2012).
[8] A. N. Nateprov, V. Ch. Kravtsov, V. Fritsch, and H. von Lohneysen, Surf. Eng. Appl. Electrochem. **47**, 540 (2011).
[9] M. Krause and F. Bechstedt, J. Supercond. Nov. Magn. **26**, 1963 (2013).
[10] T. Chonan, A. Yamada, and K. Motizuki, J. Phys. Soc. Jpn. **60**, 1638 (1991).
[11] *International Tables for Crystallography, Volume A: Space-group Symmetry*, edited by Theo Hahn, 5th Ed. (Kluwer Academic, Dordrecht, Boston, London, 2002).
[12] G. Kresse and D. Joubert, Phys. Rev. B **59**, 1758 (1999).
[13] S. H. Vosko, L. Wilk, and M. Nusair, Can. J. Phys. **58**, 1200 (1980).
[14] J. P. Perdew, K. Burke, and M. Ernzerhof, Phys. Rev. Lett. **78**, 1396 (1997).
[15] S. L. Dudarev, G. A. Botton, S. Y. Savrasov, C. J. Humphreys, and A. P. Sutton, Phys. Rev. B **57**, 1505 (1998).
[16] I. Turek, V. Drchal, J. Kudrnovský, M. Sob, and P. Weinberger, *Electronic Structure of Disordered Alloys, Surfaces and Interfaces* (Kluwer, Boston, 1997).
[17] K. Carva, J. Kudrnovský, F. Máca, V. Drchal, I. Turek, P. Baláz, V. Tkáč, V. Holý, V. Sechovský, and J. Honolka, Phys. Rev. B **93**, 214409 (2016).
[18] K. Carva, I. Turek, J. Kudrnovský, and O. Bengone, Phys. Rev. B **73**, 144421 (2006).
[19] I. Turek, J. Kudrnovský, V. Drchal, L. Szunyogh, and P. Weinberger, Phys. Rev. B **65**, 125101 (2002).
[20] A. I. Liechtenstein, M. I. Katsnelson, V. P. Antropov, and V. A. Gubanov, J. Magn. Magn. Mater. **67**, 65 (1987).
[21] I. Turek, J. Kudrnovský, V. Drchal, and P. Bruno, Philos. Mag. **86**, 1713 (2006).
[22] B. L. Gyorffy, A. J. Pindor, J. Staunton, G. M. Stocks, and H. Winter, J. Phys. F: Met. Phys. **15**, 1337 (1985).
[23] K. Binder and D. W. Heermann, *Monte Carlo Simulation in Statistical Physics* (Springer, Berlin, 1997).
[24] V. Novák (private communication).
[25] B. Alling, S. Shallcross, and I. A. Abrikosov, Phys. Rev. B **73**, 064418 (2006).
[26] F. Máca, J. Kudrnovský, V. Drchal, I. Turek, O. Stelmakhovych, P. Beran, A. Llobet, and X. Martí, Phys. Rev. B **94**, 094407 (2016).
[27] C. G. Van de Walle and J. Neugebauer, J. Appl. Phys. **95**, 3851 (2004).
[28] S. Kirklin, J. E. Saal, B. Meredig, A. Thompson, J. W. Doak, M. Aykol, S. Rühl, and C. Wolverton, npj Comput. Mater. **1**, 15010 (2015).
[29] OQMD employs 29-atoms structure for Mn but the present energy (−8.99 eV) compares well with the tabulated one (−9.03 eV) in Ref. [28].
[30] J. Kudrnovský, V. Drchal, I. Turek, S. Khmelevskyi, J. K. Glasbrenner, and K. D. Belashchenko, Phys. Rev. B **86**, 144423 (2012).
[31] C. Frontera (private communication).
[32] B. Skubic, J. Hellsvik, L. Nordström, and O. Eriksson, J. Phys.: Condens. Matter **20**, 315203 (2008).
[33] We have tested the robustness of the estimation of the Néel temperature with the respect to the size of the three-dimensional supercell. The choice 20 × 20 × 20 gives the Néel temperature 500 K.